Note added on November 9, 2022: Some figures in this document have been altered from the version originally published. The authors were alerted to unintentional duplications of PXRD patterns in figures S3, S5, S6, and S15. The corrected data is now presented herein. This change does not affect the conclusions of the paper. The authors apologise for any confusion this may have caused.

Table S1. Partial crystal data of the complex

Identification code	Complex
Empirical formula	$C_{16}H_7Cu_2O_{11}$
Formula weight	502.32
Crystal system	monoclinic
Space group	$P2_1/n$
a[Å]	10.860
b[Å]	18.909
c[Å]	14.779
α[o]	90
β[o]	92.130
γ[o]	90
V($Å^3$)	3032.797
Z	4
F(000)	996.00
T(K)	296(2)
Dcalcd, g / cm^{-3}	1.100
μ (mm^{-1})	1.438
reflections measured	3.5° ≤ 2 θ ≤ 49.99°
h,k,l	-12 ≤ h ≤ 11, -22 ≤ k ≤ 18, -17 ≤ l ≤ 17
Data completeness	0.987
unique	5262 [Rint = 0.1635]
Final R indices (I > 2 σ (I))	R1 = 0.1448
R indices (all data)	wR2 = 0.2983

CCDC	2173080
Goodness-of-fit on F^2	1.017

$^aR_1 = \sum||F0| - |Fc||/\sum|F0|$. $^bwR_2 = [\sum w (F0_2 - Fc_2)_2/\sum w (F0_2)_2]^{1/2}$

Table S2. Bond Lengths of Cu-MOF

Atom	**Length/Å**	**Atom**	**Length/Å**
Cu(1)-Cu(2)[1]	2.638(3)	Cu(2)-O(7)[6]	1.960(9)
Cu(1)-O(1)	2.154(12)	Cu(2)-O(9)	1.960(9)
Cu(1)-O(3)	1.872(12)	Cu(2)-O(10)	2.124(11)
Cu(1)-O(5)[2]	1.946(12)	O(2)-Cu(2)[1]	1.947(13)
Cu(1)-O(6)[3]	1.988(9)	O(4)-Cu(2)[7]	2.000(12)
Cu(1)-O(8)[1]	2.007(8)	O(5)-Cu(1)[8]	1.946(12)
Cu(2)-Cu(1)[4]	2.638(3)	O(6)-Cu(1)[3]	1.988(9)
Cu(2)-O(2)[4]	1.947(13)	O(7)-Cu(2)[9]	1.960(9)
Cu(2)-O(4)[5]	2.000(12)	O(8)-Cu(1)[4]	2.007(8)

[1]1/2-X, 1/2-Y, 1-Z; [2]1-X, 1-Y, 2-Z; [3]1/2+X, 1/2-Y, 1/2+Z; [4]1-X,+Y, 3/2-Z; [5]+X, 1-Y,-1/2+Z

Table S3 Bond Angles of Cu-MOF

Atom	Angle/°	Atom	Angle/°
O(1)-Cu(1)-	176.6(4)	O(2)^{4}-Cu(2)-	97.0(5)
Cu(2)^{1}	185.2(3)	O(10)	83.5(3)
O(3)-Cu(1)-	97.3(5)	O(4)^{5}-Cu(2)-	98.1(5)
Cu(2)^{1}	168.7(4)	Cu(1)^{4}	86.1(3)
O(3)-Cu(1)-O(1)	87.5(5)	O(4)^{5}-Cu(2)-	88.6(5)
O(3)-Cu(1)-O(5)^{2}	90.6(5)	O(10)	97.3(4)
O(3)-Cu(1)-O(6)^{3}	183.6(3)	O(7)^{6}-Cu(2)-	84.5(3)
O(3)-Cu(1)-O(8)^{1}	93.9(5)	Cu(1)^{4}	90.4(5)
O(5)^{2}-Cu(1)-	389.4(5)	O(7)^{6}-Cu(2)-	170.6(4)
Cu(2)	189.4(5)	O(4)^{5}	92.0(4)
O(5)^{2}-Cu(1)-O(1)	181.6(3)	O(7)^{6}-Cu(2)-	176.2(4)
O(5)^{2}-Cu(1)-O(6)	96.2(5)	O(10)	125.8(9)
O(5)^{2}-Cu(1)-O(8)	164.2(4)	O(9)-Cu(2)-	125.3(9)
O(6)^{3}-Cu(1)-	182.7(3)	Cu(1)^{4}	123.2(9)
Cu(2)	99.5(5)	O(9)-Cu(2)-O(4)^{5}	125.8(9)
O(6)^{3}-Cu(1)-O(1)	81.5(3)	O(9)-Cu(2)-O(7)^{6}	125.1(8)
O(6)^{3}-Cu(1)-	164.9(5)	O(9)-Cu(2)-O(10)	121.4(7)
O(8)^{1}	89.3(5)	O(10)-Cu(2)-	123.3(7)
O(8)^{1}-Cu(1)-	89.1(5)	Cu(1)^{4}	123.1(8)
Cu(2)		C(1)-O(2)-Cu(2)^{1}	
O(8)^{1}-Cu(1)-O(1)		C(1)-O(3)-Cu(1)	
O(2)^{4}-Cu(2)-		C(8)-O(4)-Cu(2)^{7}	
Cu(1)^{4}		C(8)-O(5)-Cu(1)^{8}	
O(2)^{4}-Cu(2)-		C(15)-O(6)-	
O(4)^{5}		Cu(1)^{3}	
O(2)^{4}-Cu(2)-		C(15)-O(7)-	

O(7)^{6}	Cu(2)^{9}
O(2)^{4}-Cu(2)-O(9)	C(16)-O(8)-Cu(1)^{4}
	C(16)-O(9)-Cu(2)

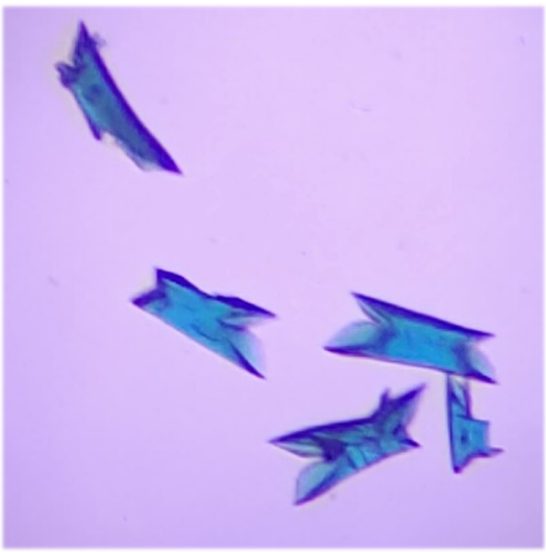

Fig. S1 The picture of crystal

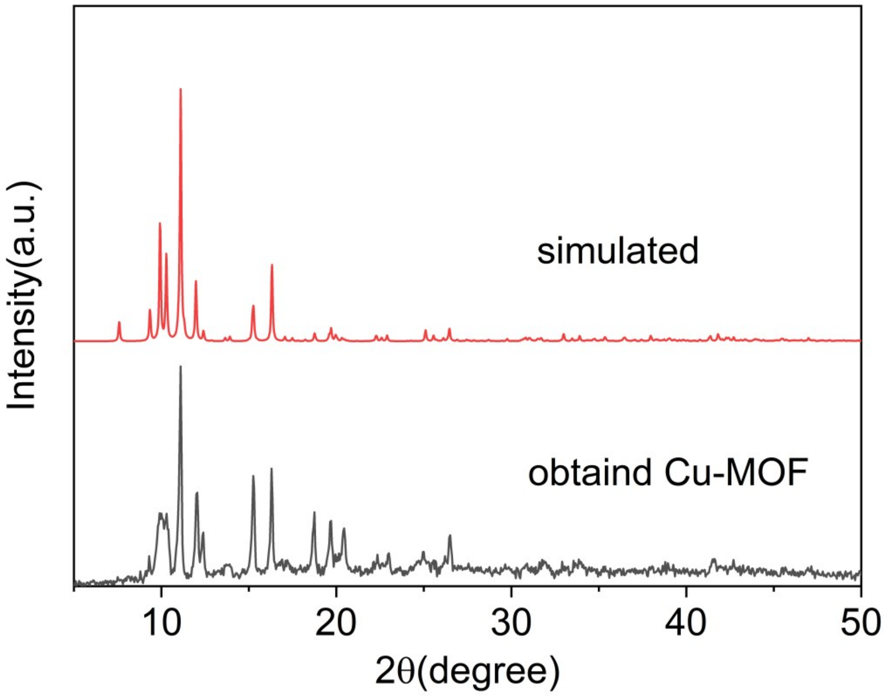

Fig. S2 The PXRD patterns of Cu-MOF

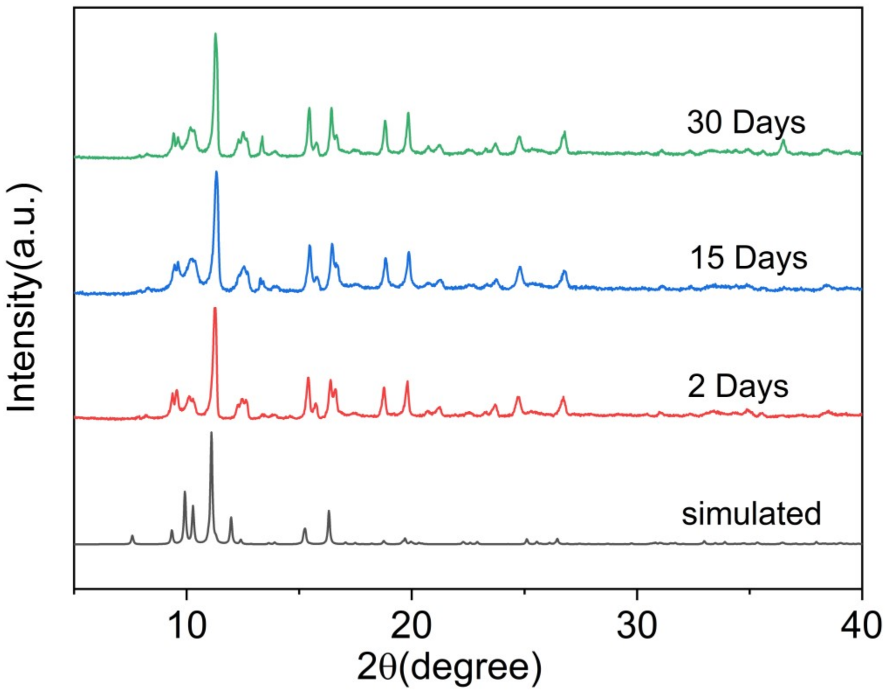

Fig. S3. PXRD patterns of Cu-MOF after immersion in water for 48 hours, 15days, 30 days

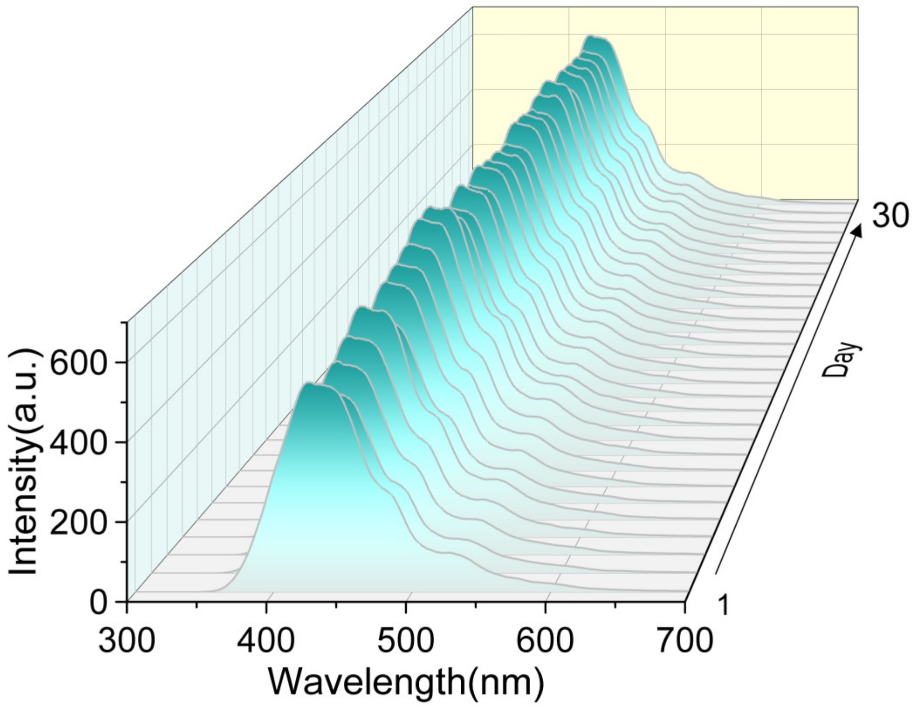

Fig. S4. Fluorescence spectra after immersion in water for 30 days

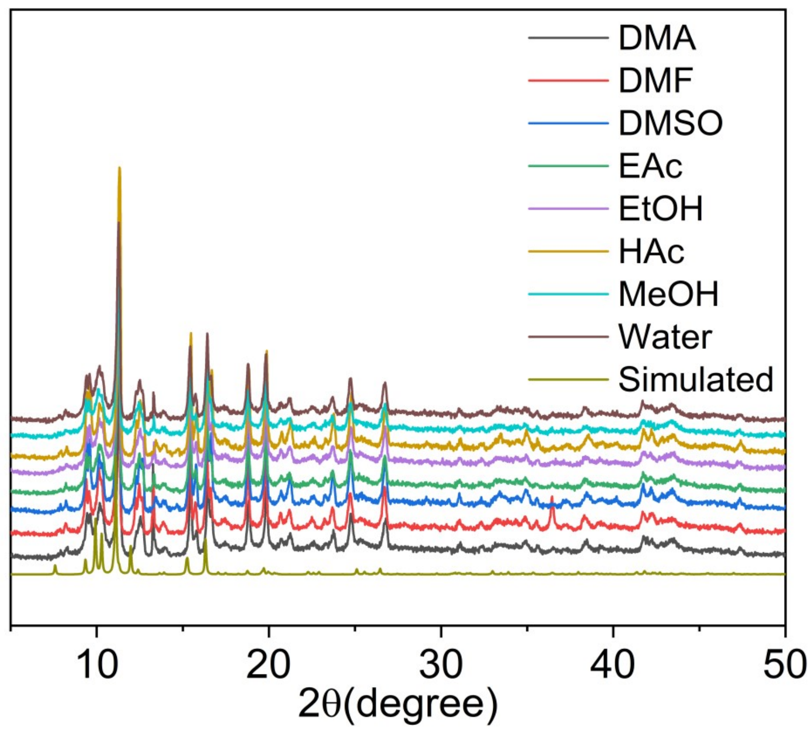

Fig. S5. The Powder X-ray diffraction patterns of compound 1 immersed in different solvents at room temperature.

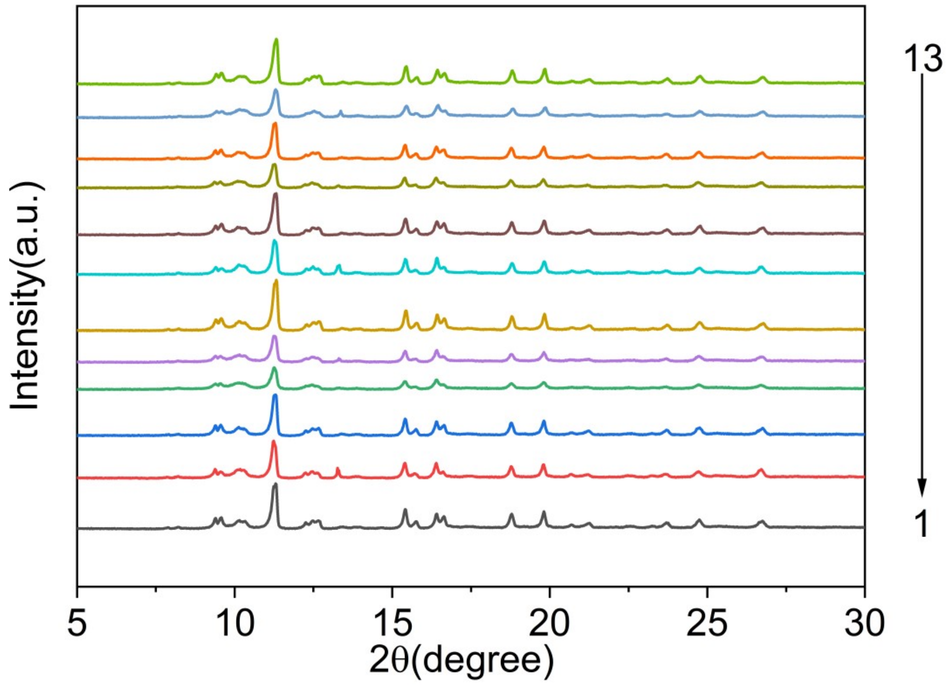

Fig. S6. PXRD patterns of Cu-MOF after immersion in pH (2-13) for 48 hours.

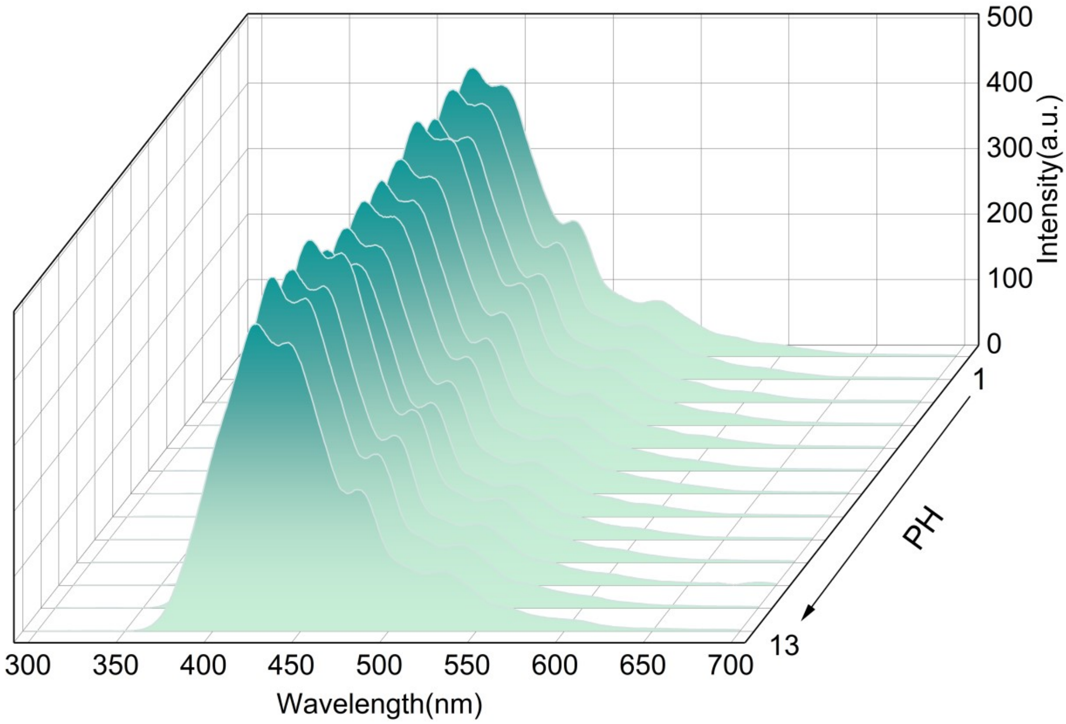

Fig. S7. Fluorescence spectra of Cu-MOF immersed in different pH for 48 hours.

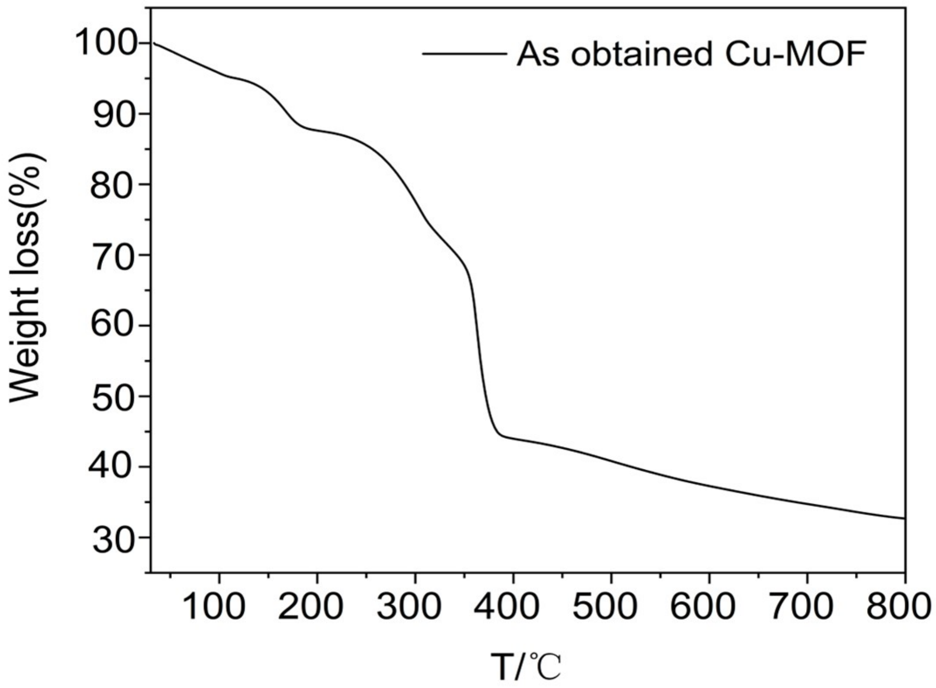

Fig. S8. The TGA curve of Cu-MOF

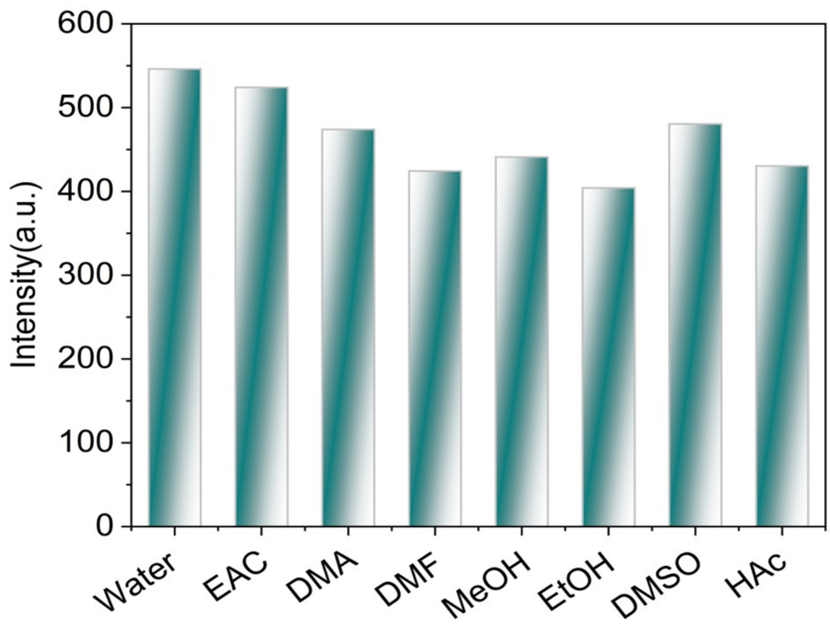

Fig. S9. Solvent selection

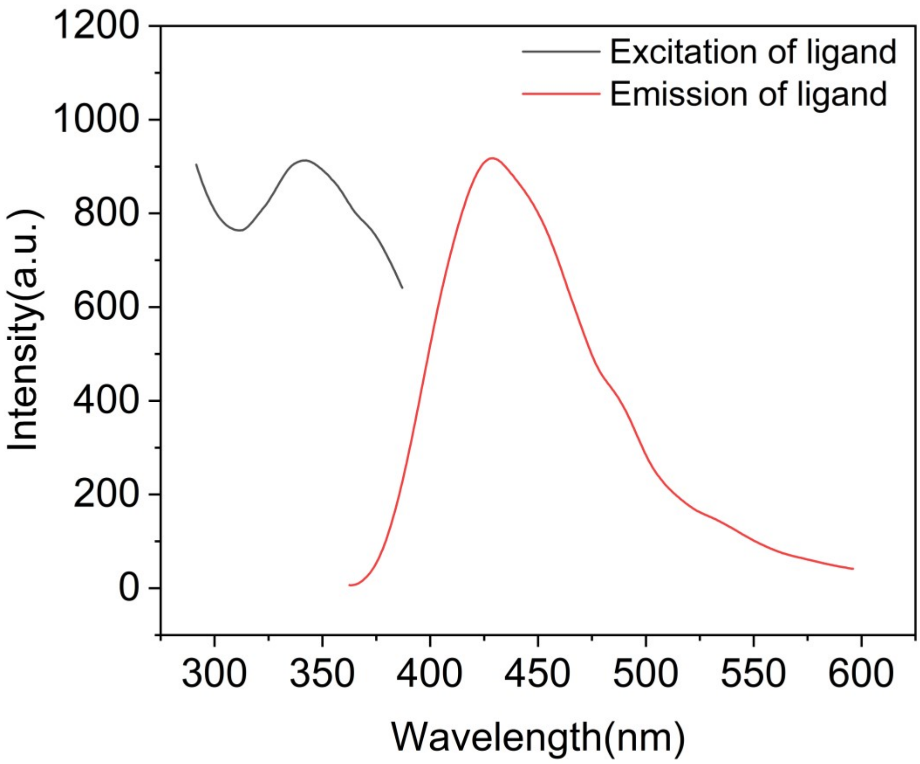

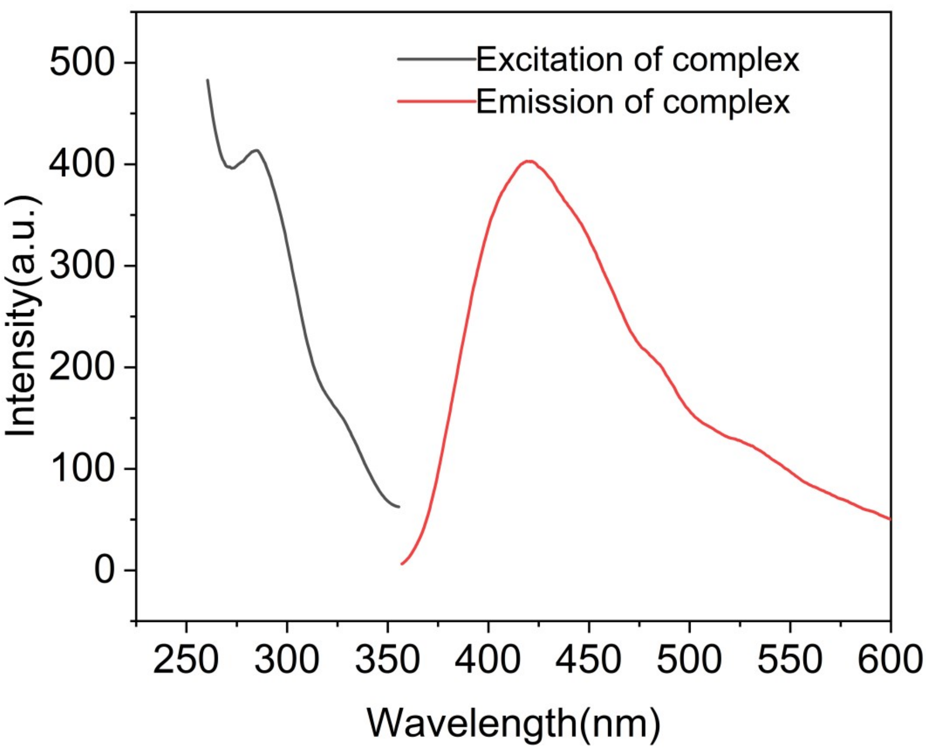

Fig. S10. Solid-state fluorescence spectra of complex and ligand .

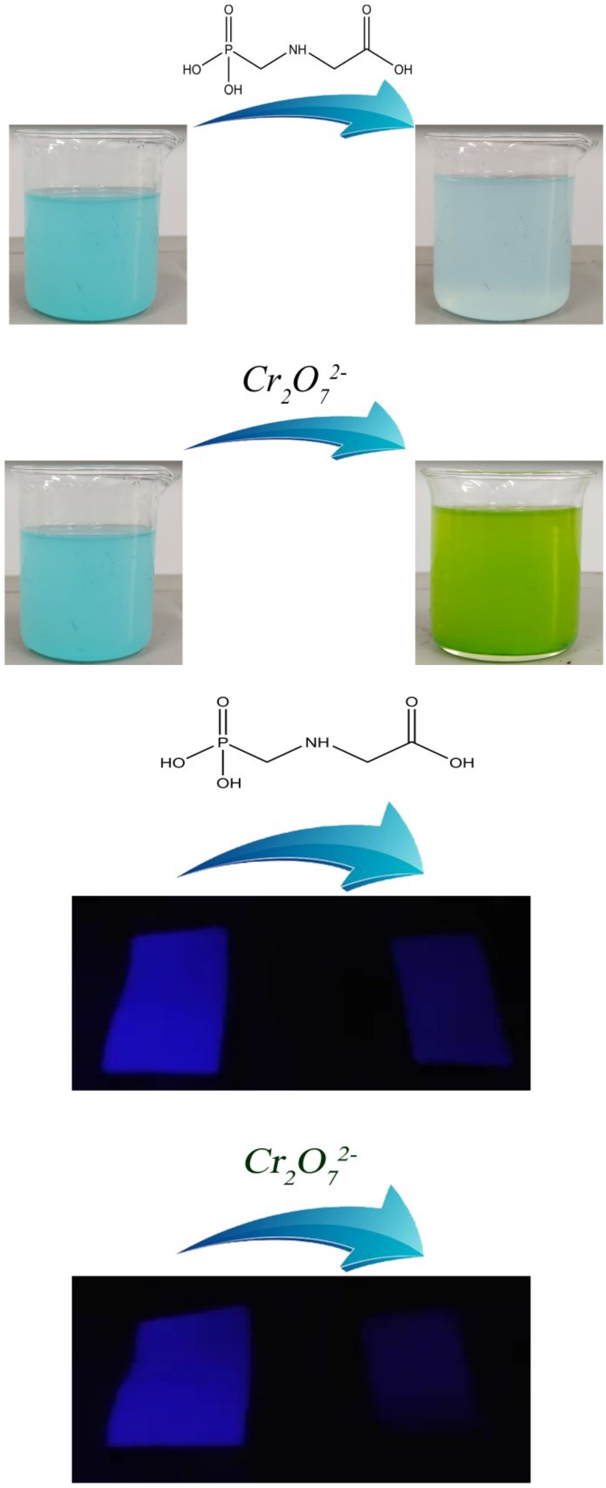

Fig. S11. Color change

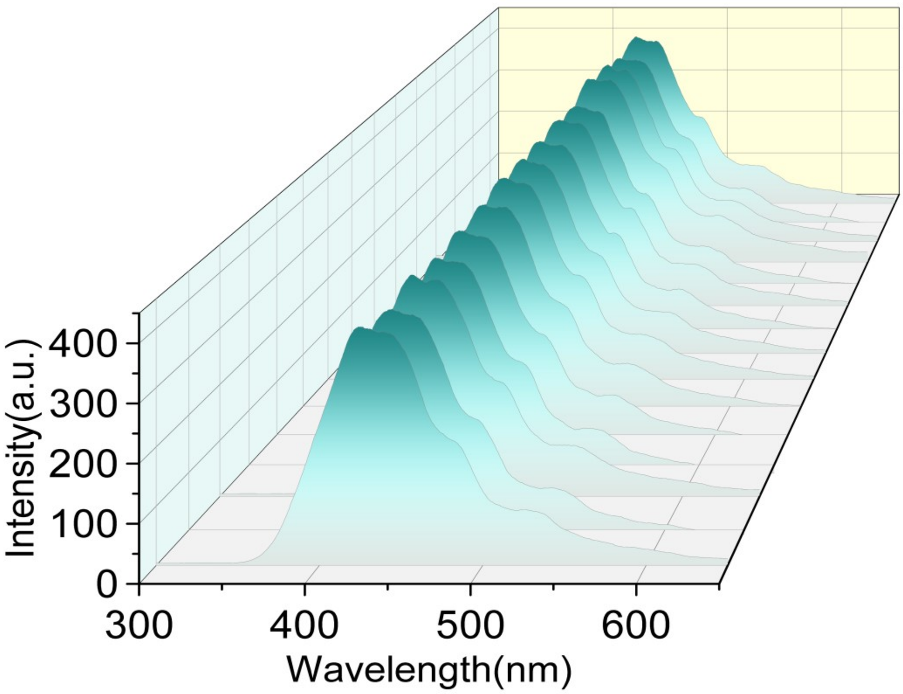

Fig. S12. Blank experiment

Table S4. Calculated detection limit

$I_0/I = K_{Sv}[Q] + b$	(1)
$LOD = 3\sigma/K_{SV}$	(2)
$\sigma = S/\ \bar{x} * 100\%$	(3)
$S = \sqrt{\frac{\sum_{i=1}^{n}(x_i - \bar{x})^2}{n-1}}$	(4)
The standard deviation is calculated according to the blank experiment	
$\bar{x}$ = 393.32	
X_i = 393.667, 393.658, 393.593, 393.57, 393.02, 392.913, 392.894, 393.063, 393.59, 393.743, 392.992, 393.97, 393.68, 393.658, 393.677 (λ_{em}=424nm)	
According to the ratio of formula 3 and 4, S = 0.353 σ= 0.09	
Glyphosate	

$I_0/I = 3.75 \times 10^3[Q] - 0.297$
According to the ratio of formula 2, LOD = 0.072 μM
$Cr_2O_7^{2-}$
$I_0/I = 2.701 \times 10^3[Q] - 0.2144$
According to the ratio of formula 2, LOD = 0.099 μM

Table S5. A comparison of limit of detection (LOD) of various sensors for sensing glyphosate (Glyp)

Sensor	Analyst	LOD [μM]	Ref.
Uio-67/Ce-PC	Glyp	0.0062	[1]
Uio-67	Glyp	0.0236	[1]
$[Tb(L)_2NO_3]_n$	Glyp	0.0144	[2]
3D $\{[Cd_2(5\text{-}NO_2\text{-}BDC)_2L(MeOH)]\cdot 2MeOH\}_n$	Glyp	31.9	[3]
2D $\{[Cd_2(5\text{-}NO_2\text{-}BDC)_2L(MeOH)]\cdot 2MeOH\}_n$	Glyp	2.25	[3]
Fe3O4@SiO2@UiO-67	Glyp	0.093	[4]
[Cd(NH2-bdc)(azp)]·DMF	Glyp	0.025	[5]
CuOx@mC composite	Glyp	$7.69*10^{-10}$	[6]
Cu-BTC MOF	Glyp	$1.4*10^{-7}$	[7]
Cu-BTC MOF/g-C_3N_4	Glyp	$1.3*10^{-7}$	[8]
Co-H_2ABDC MOF	Glyp	0.00023	[9]

$[Cu_2(H_4L)(H_2O)_2]_n$	Glyp	0.072	This work

Table S6. A comparison of limit of detection (LOD) of various sensors for sensing $Cr_2O_7^{2-}$

Sensor	Analyst	LOD [μM]	Ref
$[Ni_2(\mu_2$-OH)(azdc)(tpim)](NO_3).6DMA.6MeOH	$Cr_2O_7^{2-}$	0.95	[10]
UiO-66-NH2@eosin Y composite	$Cr_2O_7^{2-}$	0.0223	[11]
[Zn(byia)(DMF)]·1.5DMF·7H2O	$Cr_2O_7^{2-}$	1.04	[12]
$[(CH_3)_2NH_2][In(TNB)_{4/3}]\cdot(2DMF)(3H_2O)$	$Cr_2O_7^{2-}$	0.079	[13]
$[Zn_7(TPPE)_2(SO_4^{2-})_7](DMF\cdot H_2O)$	$Cr_2O_7^{2-}$	0.0926	[14]
$[Eu_2(tpbpc)_4\cdot CO_3\cdot 4H_2O]$·DMF·solvent	$Cr_2O_7^{2-}$	0.34	[15]
$[Eu(L)(HCOO)(H_2O)]n$	$Cr_2O_7^{2-}$	1.23	[16]
$[Cd\text{-}1.5(L)(2)(bpy)(NO_3)]$	$Cr_2O_7^{2-}$	0.39	[17]
$[Cu_2(H_4L)(H_2O)_2]n$	$Cr_2O_7^{2-}$	0.099	This work

Supplementary references

[1] Y. Qiang, W. Yang, X. Zhang, X. Luo, W. Tang, T. Yue and Z. Li, *Microchimica Acta*, 2022, **189**, 1-11.

[2] Y. Li, S. Wu, Y. Zhang, Z. Ma, M. Zhu and E. Gao, *Inorganica Chimica Acta*, 2021, **528**, 120632.

[3] C.-X. Yu, F.-L. Hu, J.-G. Song, J.-L. Zhang, S.-S. Liu, B.-X. Wang, H. Meng, L.-L. Liu and L.-F. Ma, *Sensors and Actuators B: Chemical*, 2020, **310**, 127819.

[4] Q. Yang, J. Wang, X. Chen, W. Yang, H. Pei, N. Hu, Z. Li, Y. Suo, T. Li and J. Wang, *Journal of Materials Chemistry A*, 2018, **6**, 2184-2192.

[5] T. Wiwasuku, J. Boonmak, R. Burakham, S. Hadsadee, S. Jungsuttiwong, S. Bureekaew, V. Promarak and S. Youngme, *Inorganic Chemistry Frontiers*, 2021, **8**, 977-988.

[6] C. Gu, Q. Wang, L. Zhang, P. Yang, Y. Xie and J. Fei, *Sensors and Actuators B: Chemical*, 2020, **305**, 127478.

[7] Y. Cao, L. Wang, C. Shen, C. Wang, X. Hu and G. Wang, *Sensors and Actuators B: Chemical*, 2019, **283**, 487-494.

[8] Y. Cao, L. Wang, C. Wang, X. Hu, Y. Liu and G. Wang, *Electrochimica Acta*, 2019, **317**, 341-347.

[9] N. Gokila, K. Muthumalai, Y. Haldorai and R. T. R. Kumar, *Chemical Physics Letters*, 2022, **795**, 139481.

[10] R. Goswami, N. Seal, S. R. Dash, A. Tyagi and S. Neogi, *ACS applied materials & interfaces*, 2019, **11**, 40134-40150.

[11] C. Gogoi and S. Biswas, *Dalton Transactions*, 2018, **47**, 14696-14705.

[12] Y. Wan, X.-M. Chen, Q. Zhang, H.-B. Jiang and R. Feng, *Designed Monomers and Polymers*, 2021, **24**, 218-225.

[13] H.-R. Fu, Y. Zhao, T. Xie, M.-L. Han, L.-F. Ma and S.-Q. Zang, *Journal of Materials Chemistry C*, 2018, **6**, 6440-6448.

[14] X.-X. Wu, H.-R. Fu, M.-L. Han, Z. Zhou and L.-F. Ma, *Crystal Growth & Design*, 2017, **17**, 6041-6048.

[15] J. Liu, G. Ji, J. Xiao and Z. Liu, *Inorganic Chemistry*, 2017, **56**, 4197-4205.

[16] Z. Sun, M. Yang, Y. Ma, L. C. Li, *Cryst. Growth Des.*, 2017, **17**, 4326−4335.

[17] M. Singh, G. Kumar and S. Neogi, *Frontiers in chemistry*, 2021, **9**.

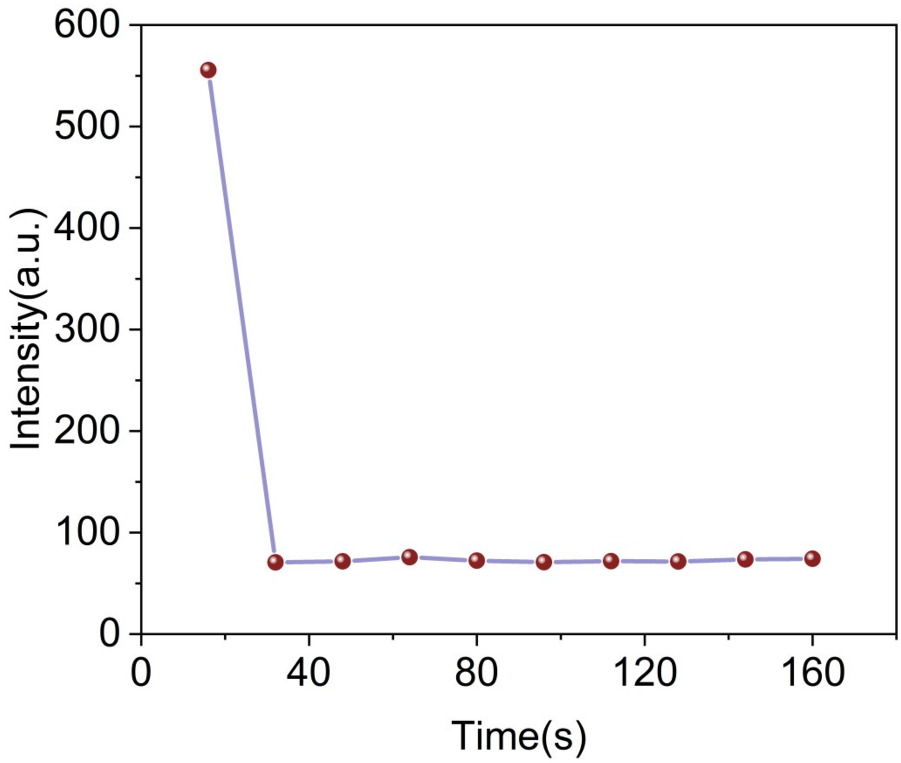

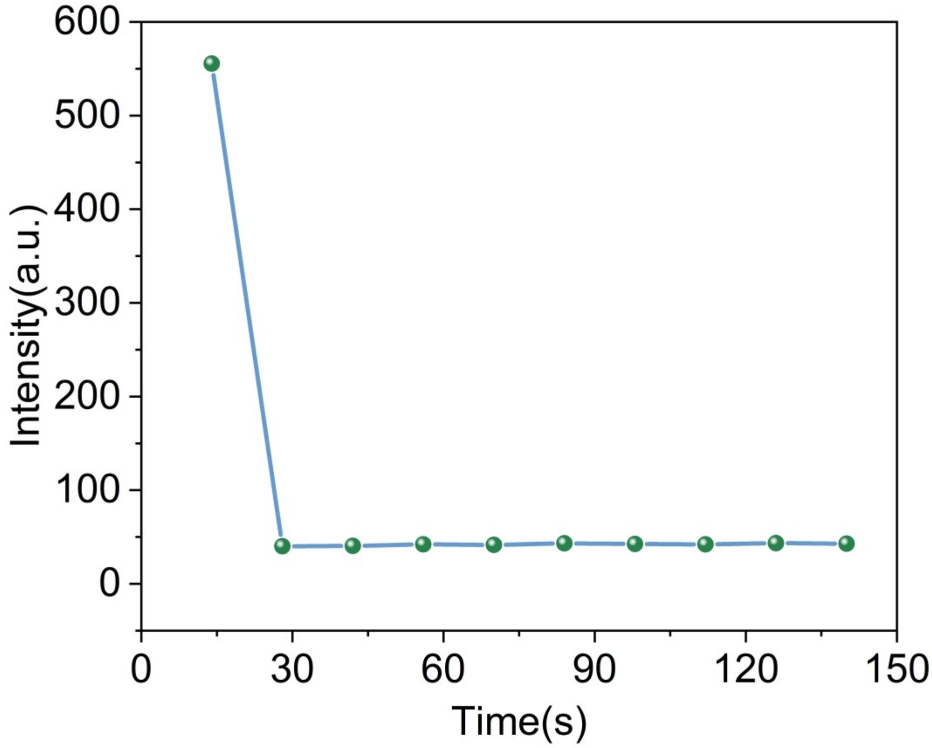

Fig. S13. Photo response time

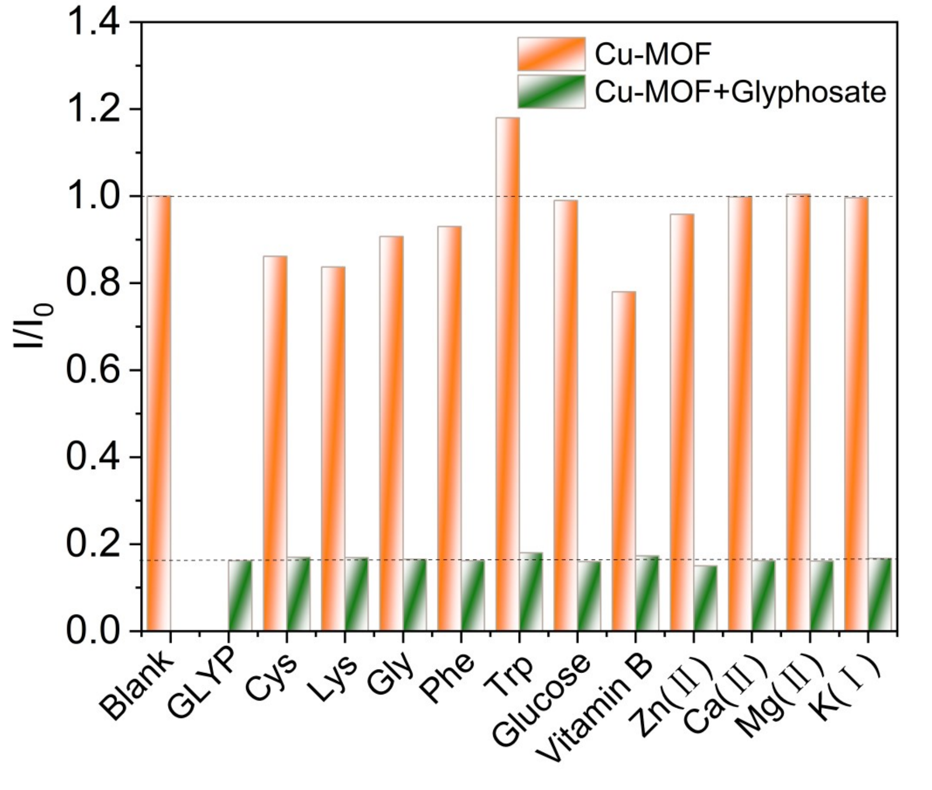

Fig. S14. The selectivity and anti-interference ability of Cu-MOF sensor (3 mg mL^{-1}) toward glyphosate (0.056 mg mL^{-1}) with interfering species.

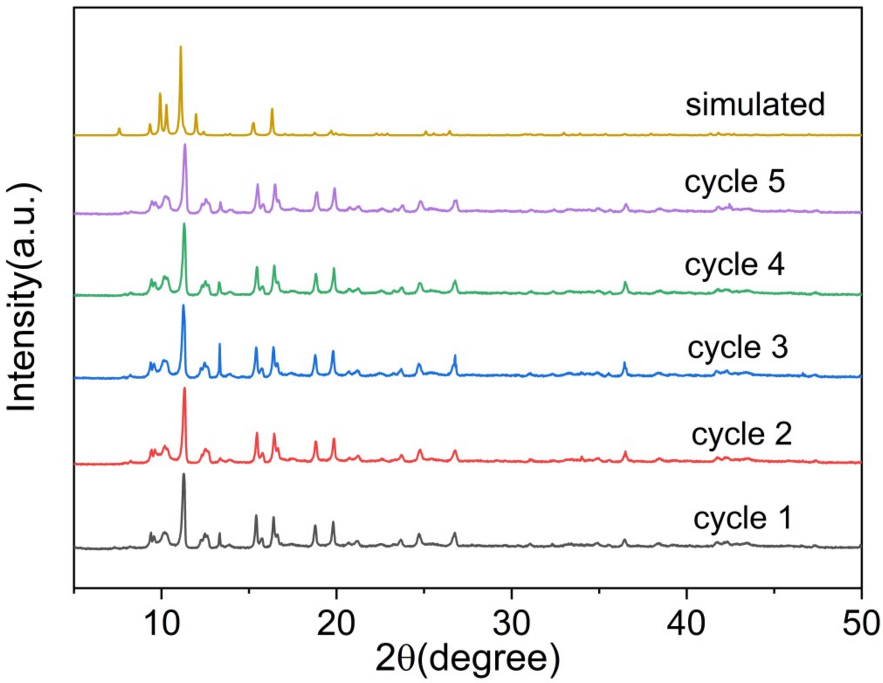

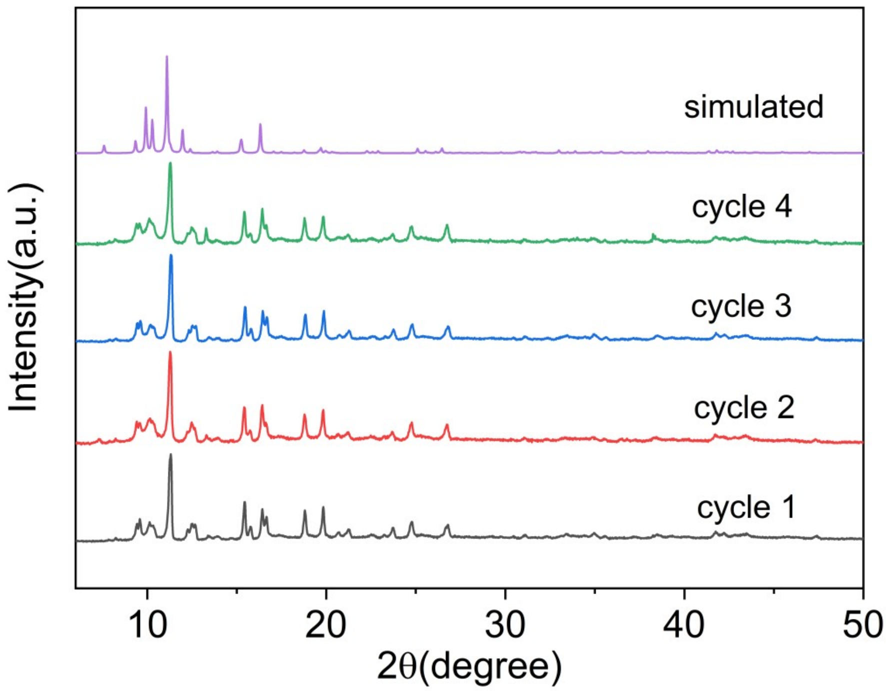

Fig. S15. The PXRD patterns of the complex after using recycles

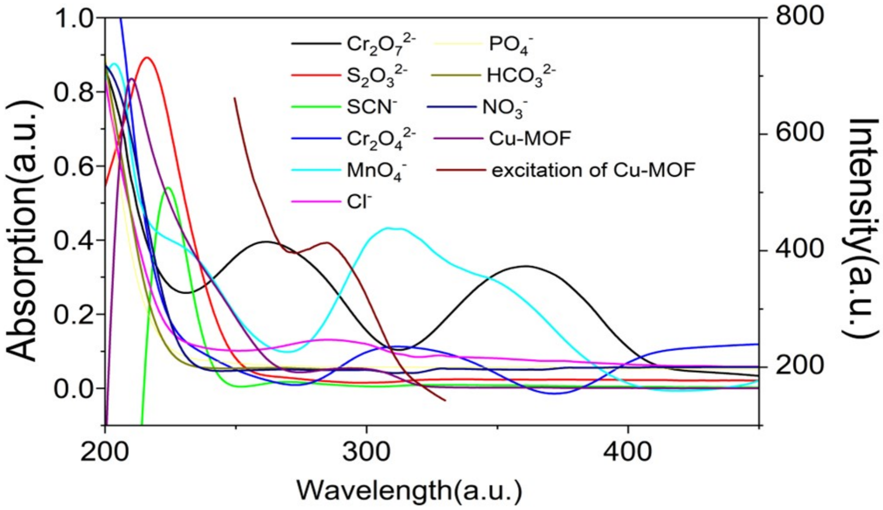

Fig. S16. Spectral overlap between the excitation spectrum of the complex and the absorption spectrum of different anions

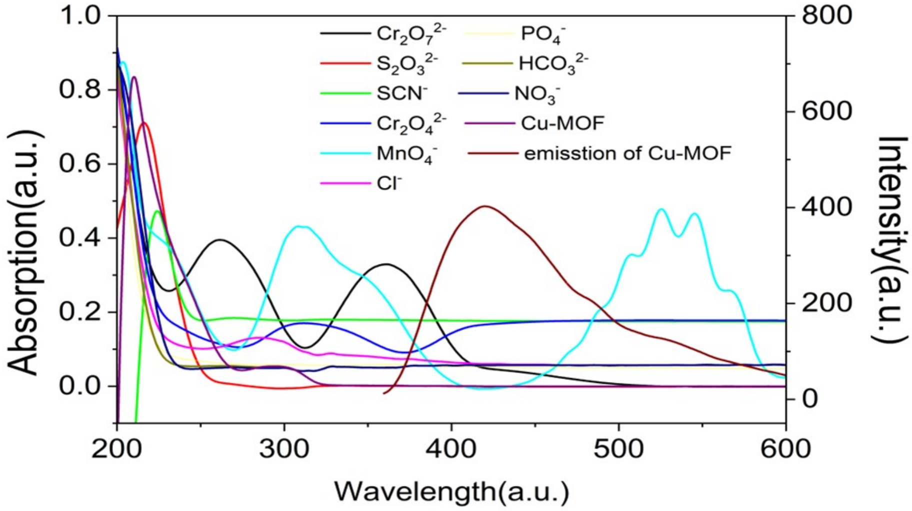

Fig. S17. Spectral overlap between the emission spectrum of the complex and the absorption spectrum of different anions

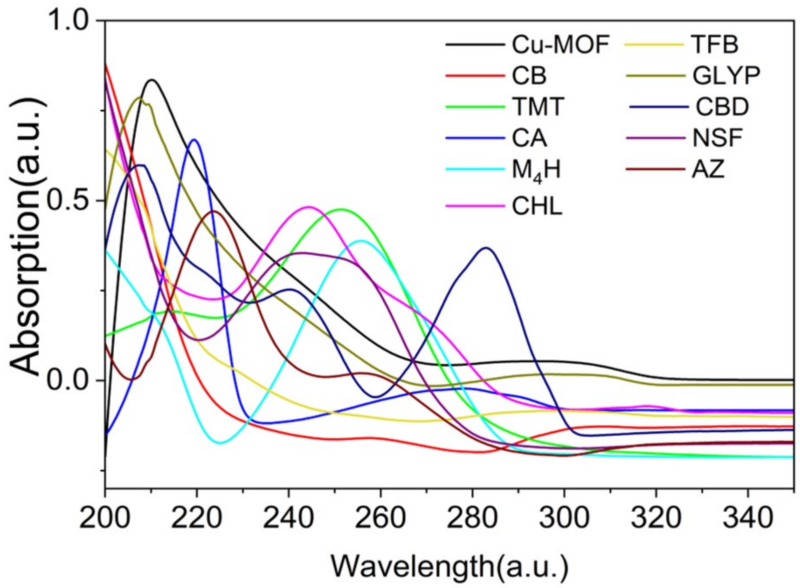

Fig. S18. Pesticides UV spectrum

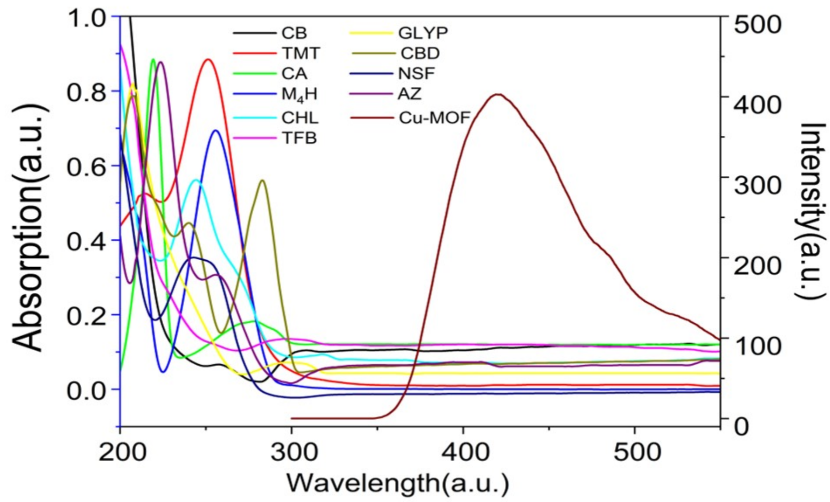

Fig. S19. Seen the emission spectrum of the complex and the absorption spectrum of different pesticides

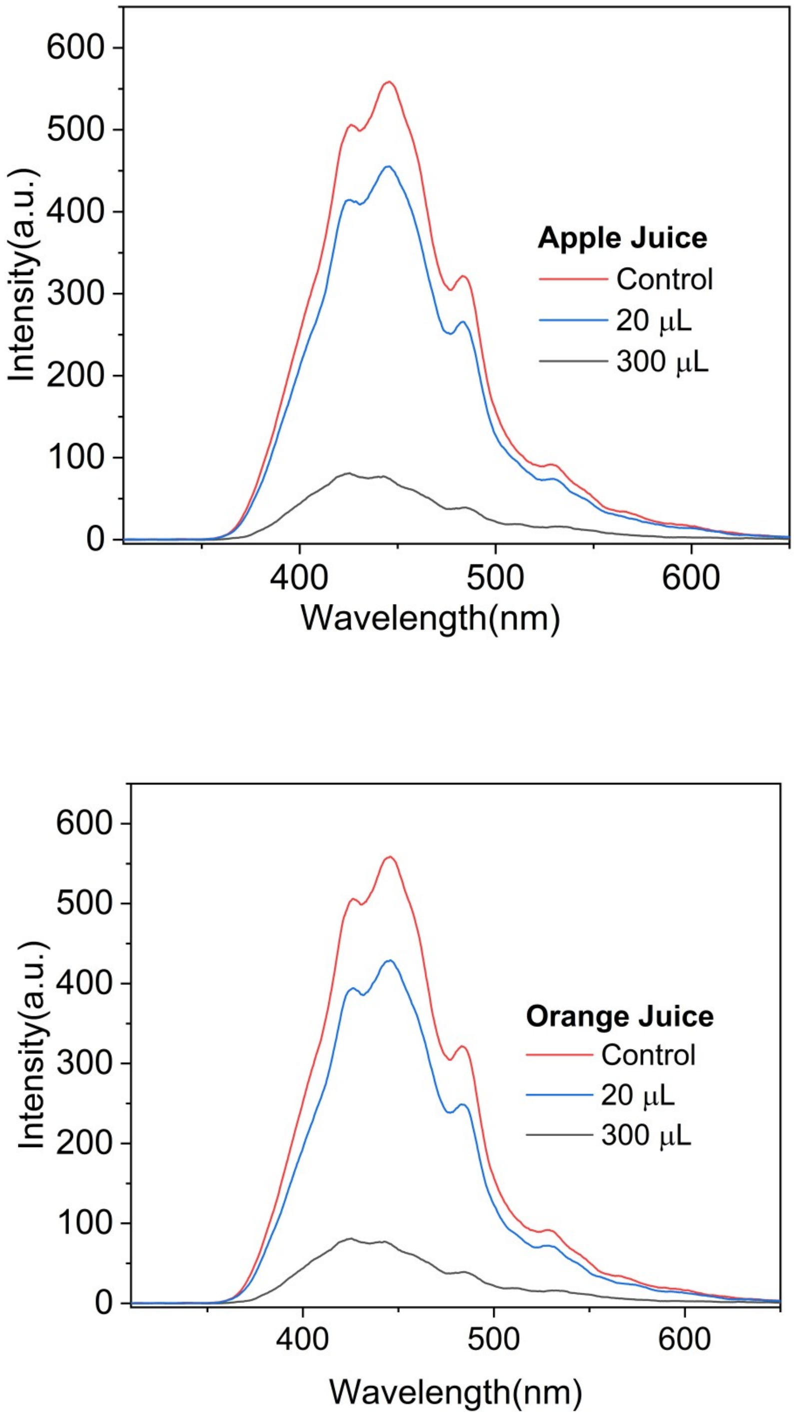

Fig. S20. The luminescence intensity of Cu-MOF in different samples

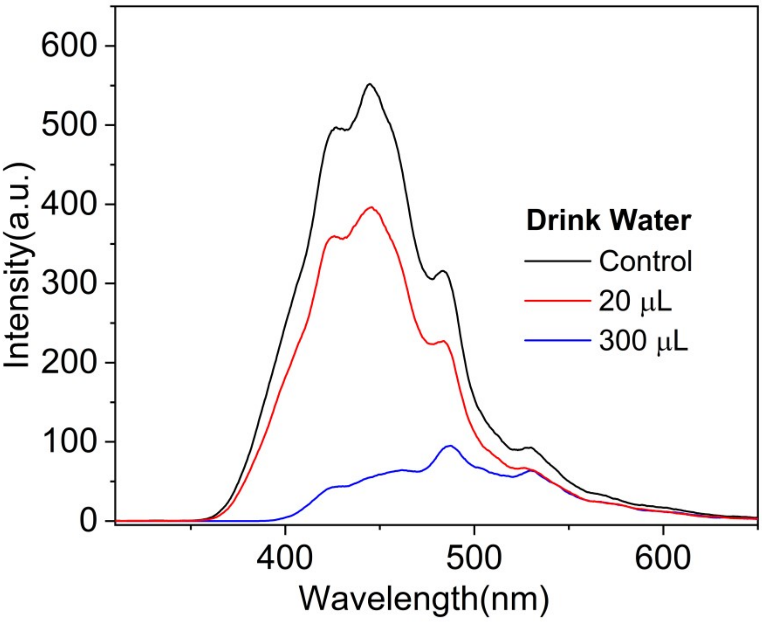
Drink Water
Control
20 μL
300 μL
Intensity(a.u.)
Wavelength(nm)
0
100
200
300
400
500
600
400
500
600

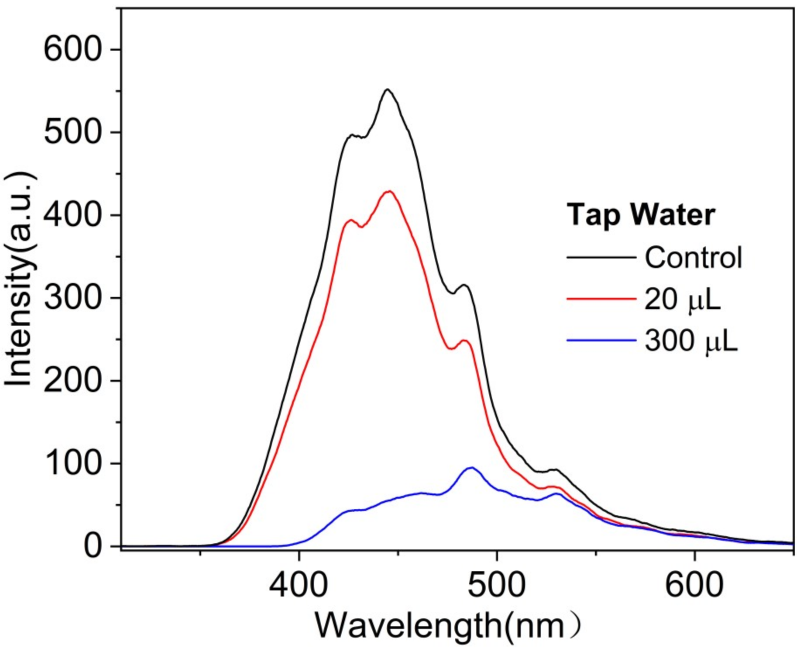
Tap Water
Control
20 μL
300 μL
Intensity(a.u.)
Wavelength(nm）
0
100
200
300
400
500
600
400
500
600

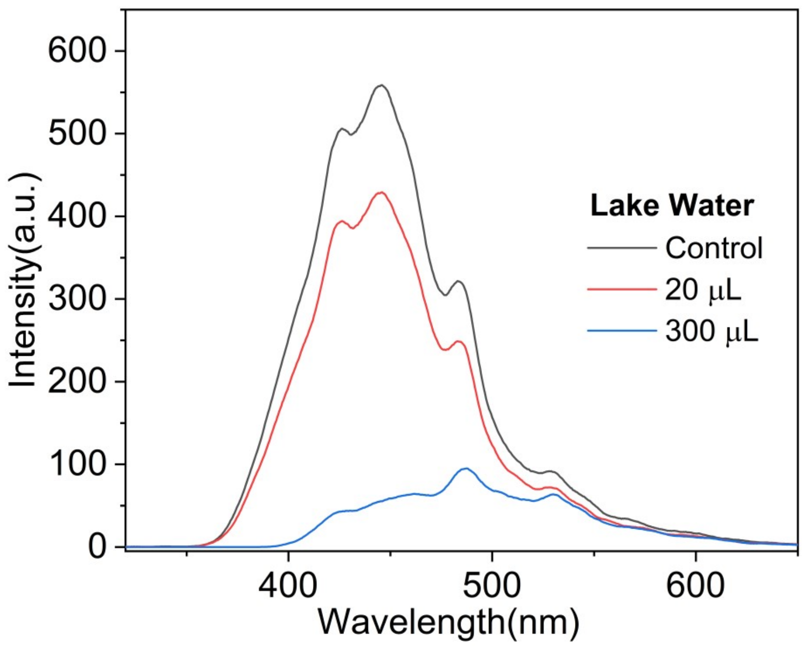

Fig. S21. The luminescence intensity of Cu-MOF in different water conditions

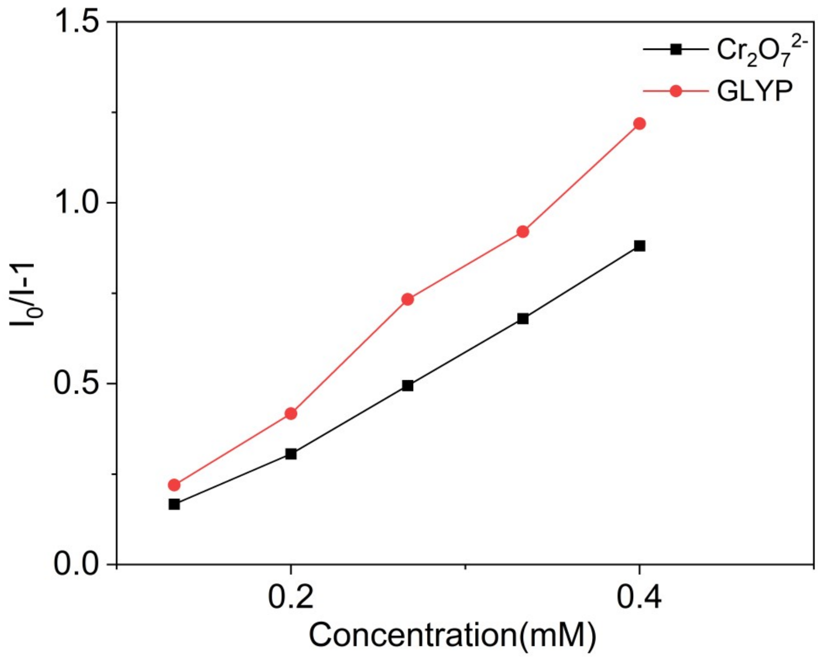

Fig. S22. Concentration fitting curve comparison